

Velocity of electroweak bubble walls

Ariel Mégevand* and Alejandro D. Sánchez†

IFIMAR (CONICET-UNMdP),

Departamento de Física, Facultad de Ciencias Exactas y Naturales, UNMdP,

Deán Funes 3350, (7600) Mar del Plata, Argentina

October 30, 2018

Abstract

We study the velocity of bubble walls in the electroweak phase transition. For several extensions of the Standard Model, we estimate the friction and calculate the wall velocity, taking into account the hydrodynamics. We find that deflagrations are generally more likely than detonations. Nevertheless, for models with extra bosons, which give a strongly first-order phase transition, the deflagration velocity is in general quite high, $0.1 \lesssim v_w \lesssim 0.6$. Therefore, such phase transitions may produce an important signal of gravitational waves. On the other hand, models with extra fermions which are strongly coupled to the Higgs boson may provide a strongly first-order phase transition and small velocities, $10^{-2} \lesssim v_w \lesssim 10^{-1}$, as required by electroweak baryogenesis.

1 Introduction

The electroweak phase transition may give rise to a variety of cosmological relics such as the baryon asymmetry of the universe, cosmic magnetic fields, inhomogeneities or gravitational waves. To be observable, some of these relics depend on the strength of the phase transition. This is the case, e.g., of the baryon asymmetry of the Universe (BAU) and gravitational waves (GWs). Both can be generated in the electroweak phase transition, and both require a strongly first-order phase transition. In a first-order phase transition,

*Member of CONICET, Argentina. E-mail address: megevand@mdp.edu.ar

†Member of CONICET, Argentina. E-mail address: sanchez@mdp.edu.ar

bubbles of the stable broken-symmetry phase nucleate at a temperature T_n below the critical temperature T_c , and grow inside the supercooled symmetric phase. The expansion of bubbles provides the required departure from thermal equilibrium.

Gravitational waves are generated by the collisions of bubble walls and by the turbulence they produce [1, 2]. As a consequence, bubble walls with higher velocities will generate GWs of larger amplitudes. For electroweak baryogenesis [3], the violation of baryon number must be suppressed in the broken-symmetry phase in order to avoid the wash-out of the generated BAU. This puts a condition on the vacuum expectation value (VEV) of the Higgs field in that phase, namely, $\langle\phi\rangle/T \gtrsim 1$. This quantity is the order parameter of the phase transition, and the above condition implies that the phase transition must be strongly first-order. The amplitude of the baryon asymmetry also depends on the wall velocity. However, unlike the case of gravitational waves, the BAU has a maximum for wall velocities in the range $v_w \sim 10^{-2} - 10^{-1}$, depending on the model [4, 5]. For higher velocities the sphaleron processes do not have enough time to produce baryons, whereas for lower velocities equilibrium is restored and the generated baryon number is washed-out. The low velocities required for baryogenesis seem to be too small to generate observable gravitational radiation.

For baryogenesis calculations the wall velocity is often assumed to be of the form [4, 5, 6, 7, 8, 9, 10]

$$v_w \approx \Delta p(T)/\eta, \quad (1)$$

where Δp is the net pressure acting on the wall, i.e., the pressure difference between the two phases, and η is a friction coefficient. This approximation corresponds to the case of subsonic walls, which propagate as *deflagrations*. In the context of gravitational waves, on the contrary, the wall is generally assumed to propagate as a *detonation* [2, 11, 12, 13, 14, 15, 16, 17]. Furthermore, a *Jouguet* detonation is assumed, leading to a simple expression for the velocity [18],

$$v_w = \frac{\sqrt{1/3} + \sqrt{\alpha^2 + 2\alpha/3}}{1 + \alpha}, \quad (2)$$

which depends only on the parameter $\alpha = L/\rho_{\text{rad}}$, where L is the latent heat and ρ_{rad} is the energy density of radiation. Equation (2) does not depend on the friction, and the Jouguet velocity gives in fact a lower bound for the detonation velocity [19, 20]. In a recent paper [21] we investigated the wall velocity as a function of L , η , and the supercooling temperature T_n . We found that Eq. (1) is a good approximation for nonrelativistic velocities, while Eq. (2) grossly underestimates the actual detonation velocity.

The calculation of the friction coefficient η is involved. It depends on all the particle species that are present in the plasma and their interactions. An accurate computation of η thus requires considering the details of the particle content in each specific model (see e.g. [6, 7]). To compare different models it is more workable to consider approximations which depend on a few parameters. Such a simple approximation was obtained in Ref. [22] using previous results [4, 6, 7, 8, 9],

$$\eta_{\text{th}} = \sum \frac{g_i h_i^4}{\Gamma_i/T} \left(\frac{\log \chi_i}{2\pi^2} \right)^2 \frac{\phi^2 \sigma}{T} \quad (3)$$

for particles with a thermal distribution, whereas infrared bosons contribute a term [10]

$$\eta_{\text{ir}} = \sum_{\text{bosons}} \frac{g_i m_D^2 T}{32\pi L_w} \log(m_i(\phi) L_w). \quad (4)$$

In these equations, g_i is the number of degrees of freedom (d.o.f.) of species i with Higgs-dependent mass $m_i = h_i \phi$, Γ_i are interaction rates which are typically $\lesssim 10^{-1}T$, $\chi_i = 2$ for fermions and $\chi_i = m_i(\phi)/T$ for bosons, σ is the surface tension of the bubble wall, $m_D^2 \sim h_i^2 T^2$ is the Debye mass squared, and L_w is the width of the bubble wall, $L_w \approx \phi^2/\sigma$. The derivation of Eqs. (3) and (4) involves expanding the distribution functions to lowest order in m_i/T , and thus they break down for $m_i/T \gg 1$. In particular, for a squared mass of the form $m_i^2 = \mu_i^2 + h_i^2 \phi^2$, with large μ_i , the particle density in the symmetric phase will be suppressed by a Boltzmann factor $\exp(-\mu_i/T)$, and this species will not contribute to the friction.

In this paper we study the velocity of bubble walls in the electroweak phase transition for several extensions of the Standard Model (SM). For that aim, we modify Eqs. (3) and (4) to take into account more general masses $m_i(\phi)$. We also take into account the effects of hydrodynamics in order to consider both deflagration and detonation solutions. We consider several extensions of the SM, including the Minimal Supersymmetric Standard Model and extensions with singlet scalars and with heavy fermions. We also investigate the effect of cubic terms in the tree level potential.

The plan is the following. In section 2 we review the dynamics of a first-order electroweak phase transition. In section 3 we find an approximation for the friction coefficient which is valid for large as well as for small values of $m_i(\phi)/T$. In section 4 we write down the equations for the wall velocity, which we solve numerically. The result depends on several parameters, namely, the critical temperature T_c , the nucleation temperature T_n , the latent heat L , and the friction coefficient η . We compute these parameters for several models in section 5, and we calculate the wall velocity. Finally, in section 6

we discuss the implications of our results for baryogenesis and gravitational wave production in the electroweak phase transition. Our conclusions are summarized in section 7.

2 Dynamics of the electroweak phase transition

In the SM, the electroweak phase transition is only a smooth crossover. However, many extensions of the model give a first-order phase transition. For simplicity we shall consider models with a single Higgs field, or models for which considering a single Higgs provides a good approximation. Thus, our theory will consist of a tree-level potential

$$V_0(\phi) = -m^2\phi^2 + \frac{\lambda}{4}\phi^4, \quad (5)$$

for a scalar field ϕ (the background Higgs field, defined by $\langle H^0 \rangle \equiv \phi/\sqrt{2}$). The vacuum expectation value of the Higgs is given by $v = \sqrt{2/\lambda m} = 246\text{GeV}$, and λ fixes the Higgs mass, $m_H^2 = 2\lambda v^2$. Imposing the renormalization conditions that the minimum of the potential and the mass of ϕ do not change with respect to their tree-level values [23], the one-loop zero-temperature potential is given by $V(\phi) = V_0(\phi) + V_1(\phi)$, with

$$V_1(\phi) = \sum_i \frac{\pm g_i}{64\pi^2} \left[m_i^4(\phi) \left(\log \left(\frac{m_i^2(\phi)}{m_i^2(v)} \right) - \frac{3}{2} \right) + 2m_i^2(\phi)m_i^2(v) \right] + c, \quad (6)$$

where g_i is the number of d.o.f. of each particle species, $m_i(\phi)$ is the ϕ -dependent mass, and the upper and lower signs correspond to bosons and fermions, respectively. We have added a constant c such that $V(v) = 0$, so that the energy density vanishes in the true vacuum at zero temperature. In the symmetric phase we will have a false vacuum energy density, given by $\rho_\Lambda = V(0)$, which contributes to the Hubble rate during the phase transition. For particle masses of the form $m_i^2 = h_i^2\phi^2 + \mu_i^2$, we have

$$\rho_\Lambda = \left[\lambda + \sum_i \frac{\mp g_i}{32\pi^2} \left(h_i^4 - 2h_i^2 \left(\frac{\mu_i}{v} \right)^2 - 2 \left(\frac{\mu_i}{v} \right)^4 \log \left(\frac{\mu_i}{v} \right)^2 \right) \right] \frac{v^4}{4}. \quad (7)$$

The free energy is given by the finite-temperature effective potential. To one-loop order, including the resummed daisy diagrams, we have

$$\mathcal{F} = V_0(\phi) + V_1(\phi) + \mathcal{F}_1(\phi, T), \quad (8)$$

where the finite-temperature corrections are given by [24]

$$\begin{aligned} \mathcal{F}_1(\phi, T) &= \sum_i \pm \frac{g_i T^4}{2\pi^2} \int_0^\infty dx x^2 \log \left[1 \mp \exp \left(-\sqrt{x^2 + m_i^2(\phi)}/T \right) \right] \\ &+ \sum_{\text{bosons}} \frac{g_i T}{12\pi} [m_i^3(\phi) - \mathcal{M}_i^3(\phi)], \end{aligned} \quad (9)$$

where the upper sign stands for bosons, the lower sign stands for fermions, and $\mathcal{M}_i^2(\phi) = m_i^2(\phi) + \Pi_i(T)$, where $\Pi_i(T)$ are the thermal masses. The last term receives contributions from all the bosonic species except the transverse polarizations of the gauge bosons.

At high temperature the symmetry is restored, and in a certain range of temperatures, the symmetric minimum $\phi = 0$ coexists with a symmetry-breaking minimum $\phi_m(T)$. The free energy density of the unbroken-symmetry phase is given by $\mathcal{F}_u(T) = \mathcal{F}(0, T)$, whereas that of the broken-symmetry phase is given by $\mathcal{F}_b(T) = \mathcal{F}(\phi_m(T), T)$. The critical temperature is that for which $\mathcal{F}_u(T_c) = \mathcal{F}_b(T_c)$. The energy density in each phase is given by $\rho(T) = \mathcal{F}(T) - T\mathcal{F}'(T)$ (a prime indicates derivative of a function with respect to its variable), and the latent heat $L \equiv \rho_u(T_c) - \rho_b(T_c)$ is given by

$$L = T_c (\mathcal{F}'_b(T_c) - \mathcal{F}'_u(T_c)). \quad (10)$$

We define the thermal energy density $\tilde{\rho}_u$ by subtracting the vacuum energy density, $\tilde{\rho}_u = \rho_u - \rho_\Lambda$. In general, we have $\tilde{\rho}_u \approx \pi^2 g_* T^4/30$, where g_* is the number of relativistic d.o.f. The hydrodynamics of the bubble wall will depend on the parameters $\alpha_c = L/\tilde{\rho}_u(T_c)$ and $\alpha_n = L/\tilde{\rho}_u(T_n)$, where T_n is the nucleation temperature.

The nucleation of bubbles [25, 26] is governed by the three-dimensional instanton action

$$S_3 = 4\pi \int_0^\infty r^2 dr \left[\frac{1}{2} \left(\frac{d\phi}{dr} \right)^2 + V_T(\phi(r)) \right], \quad (11)$$

where

$$V_T(\phi) \equiv \mathcal{F}(\phi, T) - \mathcal{F}(0, T). \quad (12)$$

The bounce solution of this action, which is obtained by extremizing S_3 , gives the radial configuration of the nucleated bubble, assumed to be spherically symmetric. The action of the bounce coincides with the free energy of a critical bubble (i.e., a bubble in unstable equilibrium between expansion and contraction). This solution obeys the equation

$$\frac{d^2\phi}{dr^2} + \frac{2}{r} \frac{d\phi}{dr} = V'_T(\phi) \quad (13)$$

with boundary conditions

$$\frac{d\phi}{dr}(0) = 0, \quad \lim_{r \rightarrow \infty} \phi(r) = 0. \quad (14)$$

We will solve Eq. (13) iteratively by the overshoot-undershoot method¹. The thermal tunneling probability for bubble nucleation per unit volume and time is [26]

$$\Gamma_n(T) \simeq A(T) e^{-S_3(T)/T}, \quad (15)$$

with $A(T) = [S_3(T)/(2\pi T)]^{3/2}$. The nucleation time t_n is defined as that at which the probability of finding a bubble in a causal volume is 1,

$$\int_{t_c}^{t_n} dt \Gamma_n(T) V_c = 1, \quad (16)$$

where t_c is the time at which the Universe reached the critical temperature T_c and, in the radiation-dominated era, the causal volume is given by $V_c \sim (2t)^3$. The time-temperature relation is given by

$$dT/dt = -HT, \quad (17)$$

where H is the expansion rate, $H = \sqrt{8\pi G\rho_u(T)}/3$. Here, G is Newton's constant. Using Eq. (17) we can solve Eq. (16) for the temperature T_n at which the first bubbles are nucleated. If $\rho_u \approx \tilde{\rho}_u \approx \pi^2 g_* T^4/30$, then the time-temperature relation is given by the usual expression $t = \xi M_P/T^2$, where M_P is the Planck mass and $\xi = \sqrt{45/(16\pi^3 g_*)}$.

It is useful to consider the profile $\phi(r)$ of the critical bubble at $T \approx T_c$. At the critical temperature, the radius of the nucleated bubble diverges (and the nucleation rate vanishes). Hence, for $T \approx T_c$ the second term in Eq. (13) can be neglected, since the wall is much thinner than the radius. Thus, one obtains

$$d\phi/dr = -\sqrt{2V_T(\phi(r))}. \quad (18)$$

Within this approximation, the wall is planar and its surface tension $\sigma \equiv \int_{-\infty}^{+\infty} (d\phi/dr)^2 dr$ is given by

$$\sigma = \int_0^{\phi_c} \sqrt{2V_T(\phi)} d\phi, \quad (19)$$

where $\phi_c \equiv \phi_m(T_c)$. We can also invert relation (18) to obtain the wall width L_w . If we define, e.g., $L_w = r(\phi = 0.1\phi_c) - r(\phi = 0.9\phi_c)$, we have

$$L_w = \int_{0.1\phi_c}^{0.9\phi_c} d\phi / \sqrt{2V_T(\phi)}. \quad (20)$$

¹See Ref. [27] for details.

Roughly, σ and L_w are related by $\sigma \sim \phi_c^2/L_w$, and the wall width is given by $L_w \sim V_T''(0)^{-1/2}$.

3 Microphysics

According to kinetic theory, for a planar wall in stationary motion along the z direction, the friction force per unit area is given by [6]

$$\text{friction} = \sum g_i \int_{-\infty}^{+\infty} dz \int \frac{d^3p}{(2\pi)^3} \frac{dE}{dm^2} \frac{dm_i^2}{d\phi} \frac{d\phi}{dz} \delta f_i, \quad (21)$$

where $E = \sqrt{p^2 + m^2}$ and δf_i is the departure from the equilibrium distribution $f_0(E_i/T)$ for each particle species, with

$$f_0(x) = \frac{1}{e^x \pm 1}. \quad (22)$$

The kinetic description is valid for particles with $p \gg L_w^{-1}$, for which the background field varies slowly and the semiclassical (WKB) approximation is valid. Since in general $L_w^{-1} \ll T$, this condition is satisfied for all but the most infrared particles [6]. As usual, we will assume that the friction is proportional to the wall velocity,

$$\text{friction} = \eta v_w, \quad (23)$$

where the friction coefficient η is obtained by considering Eq. (21) to linear order in v_w . The deviations δf_i can in principle be calculated by considering the Boltzmann equation for the distribution functions [4, 6, 7, 8, 9]. However, infrared excitations of bosonic fields should be treated classically and undergo overdamped evolution [10, 28, 29]. We shall refer to these fields as “infrared bosons”, whereas we shall call “thermal particles” those which obey the Boltzmann equation.

3.1 Thermal particles

We begin by considering the case of thermal particles. It is usual to employ the ansatz $f = f_0(E/T - \mu/T + E\delta T/T^2 + p_z v/T)$ for the distribution functions [6, 7]. In that case, a system of equations for μ , δT and v for each particle species can be derived from the Boltzmann equation

$$[\partial_t + (\partial_{p_z} E) \partial_z - (\partial_z E) \partial_{p_z}] f = -C[f], \quad (24)$$

where $C[f]$ is the collision term. We need to simplify further the problem in order to obtain a simple analytical expression which can be applied to different models. Therefore, we shall use the ansatz $f = f_0(E/T - \delta)$, which is equivalent to considering only the term μ/T . Hence, the deviation from $f_0(E/T)$ is $\delta f = -f'_0(E/T)\delta$, and the equation for δ is obtained by linearizing the Boltzmann equation. Assuming stationary motion and making a momentum integration, one obtains, for each particle species (see Ref. [22] for details),

$$c_2 v_w \frac{d\delta}{dz} - \Gamma \delta = \frac{c_1 v_w}{2T^2} \frac{dm^2}{dz}, \quad (25)$$

where Γ is an interaction rate arising from the collision integrals, and the coefficients c_1 and c_2 are defined by

$$c_1 \equiv -\frac{1}{T^2} \int \frac{d^3p}{(2\pi)^3} \frac{f'_0(E/T)}{E}, \quad c_2 \equiv -\frac{1}{T^3} \int \frac{d^3p}{(2\pi)^3} f'_0(E/T). \quad (26)$$

It is out of the scope of this work to calculate the collision integrals, which depend on the particle content of each model. Numerically, the rates Γ are $\sim 10^{-2}T$ [6], and we shall set $\Gamma/T = 5 \times 10^{-2}$. In the thick wall limit, the first term in Eq. (25) can be neglected, and we obtain

$$\delta = -\frac{c_1 v_w}{2T^2 \Gamma} \frac{dm^2}{dz}. \quad (27)$$

We now insert $\delta f = -f'_0(E/T)\delta$ in Eq. (21), with δ given by Eq. (27), with $m^2 = \mu_i^2 + h_i^2 \phi^2$ for each particle species i . Performing the momentum integration we obtain

$$\eta = \sum_i \frac{g_i h_i^4}{\Gamma} \int_{-\infty}^{+\infty} c_{1i}^2 \phi^2 \phi'^2 dz. \quad (28)$$

For $T \approx T_c$ we can use the thin wall approximation² $\phi' = \sqrt{2V_T(\phi)}$ in Eq. (28). Thus, the friction caused by particles with thermal distributions is given by

$$\eta_{\text{th}} = \sum_i \frac{g_i h_i^4}{\Gamma} \int_0^{\phi_c} c_{1i}^2(\phi) \phi^2 \sqrt{2V_T} d\phi. \quad (29)$$

Particles with larger couplings h give the main contributions to the friction force, since they have stronger interactions with the bubble wall.

²The wall is thick in comparison with T^{-1} , but it is thin in comparison with the bubble radius.

3.2 Infrared bosons

Infrared boson excitations must be treated classically [28] and undergo overdamped evolution [29]. Relating the population function to the squared amplitude of the field [10], one obtains the equation

$$\frac{\pi m_D^2}{8p} \frac{df}{dt} = -E^2 \delta f, \quad (30)$$

where m_D^2 is the squared Debye mass, $m_D^2 = (11/6)g^2T^2$ for the W and Z bosons of the SM, and $m_D^2 = h^2T^2/3$ for a scalar singlet. Writing $f = f_0(E/T) + \delta f$ we have, to first-order in v_w ,

$$\delta f = -\frac{\pi m_D^2}{16pTE^3} f_0' \frac{dm^2}{d\phi} \phi' v_w. \quad (31)$$

Inserting the departure from equilibrium (31) in Eq. (21) and doing the momentum integration, we obtain

$$\eta = \sum_{\text{bosons}} g_i \frac{\pi m_D^2}{8T^3} h^4 \int_{-\infty}^{+\infty} b \phi^2 \phi'^2 dz. \quad (32)$$

with

$$b = -T^2 \int \frac{d^3p}{(2\pi)^3} \frac{p}{pE^4} f_0'(E/T). \quad (33)$$

The integral in Eq. (32) will diverge if $m(\phi)$ vanishes. Indeed, for small m/T , the momentum integral (33) is infrared dominated. Therefore, we can make the approximation $f_0'(x) \simeq -1/x^2$, and we obtain

$$b = T^4 / (8\pi^2 m^4). \quad (34)$$

Hence, for $\mu = 0$ the integral in Eq. (32) has a logarithmic divergence at $\phi = 0$. However, the kinetic description (21) breaks down for very infrared particles, which in the case $m \rightarrow 0$ dominate. The actual contribution of degrees of freedom with $p \lesssim L_w^{-1}$ is subdominant, because their wavelength cannot resolve the thickness of the wall [10]. Thus, for small μ we will cut off the integral at $m(\phi) = L_w^{-1}$, and we have

$$\eta_{\text{ir}} = \sum_{\text{bosons}} g_i \frac{\pi m_D^2}{8T^3} h^4 \int_{\phi_0}^{\phi_c} d\phi \phi^2 \sqrt{2V_T} b(\phi), \quad (35)$$

with $\phi_0 = \sqrt{L_w^{-2} - \mu^2}/h$ for $\mu < L_w^{-1}$, and $\phi_0 = 0$ for $\mu > L_w^{-1}$. For a particle with small enough h , we will have $\phi_0 > \phi_c$. In such a case the particle will not contribute to the friction and we shall set $\eta = 0$.

Since Eqs. (29) and (35) depend on the profile of the wall, the contribution of a particle species to the friction depends on the whole particle content of the model. As an example, we consider the case of the SM with an additional complex scalar field. Figure 1 shows the contribution of the extra singlet to the friction as a function of the coupling h . The dashed line corresponds to the friction coefficient η_{th} given by Eq. (29), the dotted line to η_{ir} given by Eq. (35), and the solid line shows their sum. In Fig. 2 we fix $h = 1$ and vary μ . The coefficients η_{th} and η_{ir} dominate in different parameter regions, and we shall use $\eta = \eta_{\text{th}} + \eta_{\text{ir}}$ for applications in this paper. As expected, η_{ir} dominates for relatively small values of μ and h . We see that the friction increases with h , as particles interact more strongly with the wall, and decreases with μ due to Boltzmann suppression of the particle density.

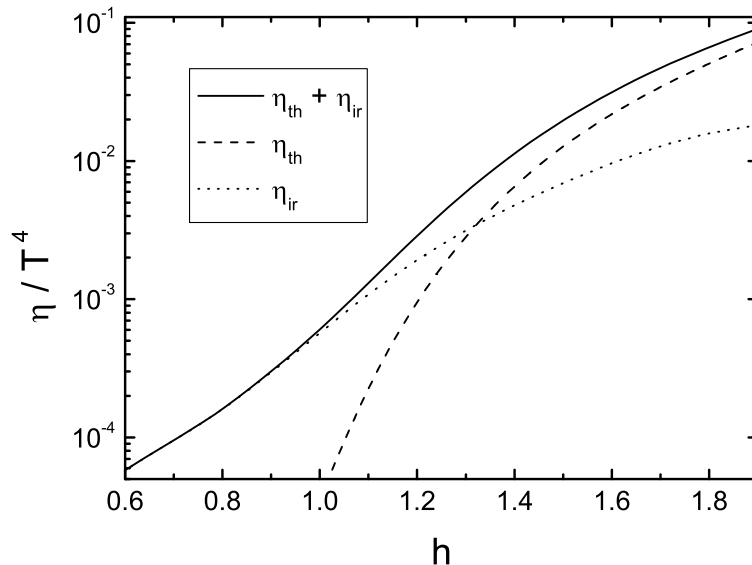


Figure 1: The contribution of a complex singlet to the friction as a function of the coupling h for $\mu = 0$ and $m_H = 125\text{GeV}$.

3.3 Limiting cases

In section 5 we shall compute the friction coefficient for each species numerically. It is useful, though, to consider here some limiting cases.

The coefficient c_1 depends on $m(\phi)$. It is usual to consider only the lowest order in m/T . In that limit we have

$$c_{1f} = \log 2/2\pi^2, \quad c_{1b} = -\log(m/T)/2\pi^2, \quad (36)$$

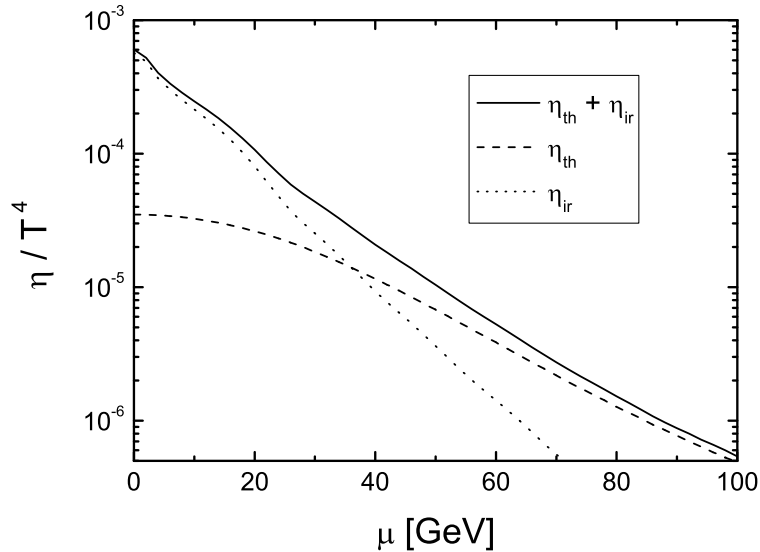


Figure 2: The contribution of a complex singlet to the friction as a function of μ for $h = 1$ and $m_H = 125\text{GeV}$.

for fermions and bosons respectively. Since c_{1b} depends only logarithmically on m , we may replace $m(\phi) \approx m(\phi_c)$ in Eq. (36). The integral in Eq. (29) goes like $\phi_c^2 \sigma$, and in the small m/T limit we recover Eq. (3),

$$\eta_{\text{th}} \sim gh^4 \frac{\phi_c^2 \sigma}{\Gamma} \left(\frac{\log \chi}{2\pi^2} \right)^2 \quad \text{for } m/T \ll 1, \quad (37)$$

with $\chi = 2$ for fermions and $\chi = \sqrt{h^2 \phi_c^2 + \mu^2}/T \sim h$ for bosons. However, the approximation (36) will break down whenever μ or $h\phi$ become large in comparison with the temperature. In particular, particles with large h in a strong phase transition will have $m \sim h\phi \gg T$ in the broken-symmetry phase.

In the limit $m/T \gg 1$ we have

$$c_1 = (m/T)^{1/2} \exp(-m/T) / (2\pi)^{3/2}. \quad (38)$$

It is apparent that the contribution of a heavy particle to the friction is suppressed by a Boltzmann factor. In the case of small μ but $h\phi_c \gg T$, we can estimate the integral in Eq. (29) using a quartic approximation for the effective potential at $T = T_c$, $V_T(\phi) \approx A\phi^2(\phi_c - \phi)^2$ with $A = V_T''(0)/(2\phi_c^2)$. Since for small ϕ the integrand is suppressed by a factor ϕ^3 , we can use the approximation (38) in Eq. (29). To leading order in $h\phi_c/T_c$, we obtain

$$\eta_{\text{th}} \approx \frac{3g}{32\pi^3} \frac{\sqrt{V_T''(0)} T_c^4}{\Gamma} \quad \text{for } h\phi_c/T_c \gg 1. \quad (39)$$

We see that in the limit of a very strong phase transition the friction coefficient does not increase like h^4 as in Eq. (37). This is because the integrand in Eq. (29) is suppressed for $h\phi \gtrsim T$. Still, η grows with the strength of the phase transition due to the factor $\sqrt{V_T''(0)}$. For a heavy particle with $\mu \gg T$, the function c_1 does not depend on ϕ , and the integral in Eq. (29) goes with $c_1^2 \phi_c^2 \sigma$. Therefore, we have

$$\eta_{\text{th}} \sim \frac{gh^4}{(2\pi)^3} \frac{\phi_c^2 \sigma}{\Gamma} \frac{\mu}{T} e^{-2\mu/T} \quad \text{for } \mu/T \gg 1. \quad (40)$$

This exponential suppression of the contribution to the friction is important, since the heavy particle will also be decoupled from the effective potential. For instance, as the value of μ for a boson is increased, the phase transition becomes weaker. Consequently, there will be less supercooling and a smaller pressure difference at $T = T_n$. Nevertheless, the wall velocity will not necessarily decrease, since the friction will also be smaller.

For the coefficient b , we have the approximation (34) for $m/T \ll 1$. For small ϕ we also have $V_T(\phi) \approx \frac{1}{2} V_T''(0) \phi^2$, and we obtain

$$\eta \approx \frac{gm_D^2 \sqrt{V_T''(0)} T_c}{64\pi} \left[\log \frac{m(\phi_c)}{m(\phi_0)} - \frac{(m^2(\phi_c) - m^2(\phi_0)) \mu^2}{2m^2(\phi_c) m^2(\phi_0)} \right] \quad \text{for } m/T \ll 1. \quad (41)$$

The factor of h^4 in (35) has disappeared, but a factor h^2 still remains in m_D^2 . This is the generalization of Eq. (4) for small but nonvanishing μ . Notice that for $\mu < L_w^{-1}$ we have $m(\phi_0) = L_w^{-1}$, while for $\mu > L_w^{-1}$ we have $m(\phi_0) = \mu$. Thus, noting that $\sqrt{V_T''(0)} \sim L_w^{-1}$, we recover Eq. (4) in the limit $\mu \rightarrow 0$. On the other hand, for $\mu \neq 0$ the friction is smaller.

In the limit of very large m/T , we have

$$b = e^{-m/T} T^3 / (2\pi^2 m^3). \quad (42)$$

Let us consider, e.g., the case $\mu = 0$ and $h\phi_c \gg T$. Since b is exponentially suppressed for $m = h\phi \gg T$, we cut off the integral in Eq. (35) at $\phi = T/h \ll \phi_c$ and use the small m approximation for b . Thus, we obtain

$$\eta \sim \frac{gm_D^2 \sqrt{V_T''(0)} T_c}{64\pi} \log(TL_w) \quad \text{for } h\phi_c/T_c \gg 1. \quad (43)$$

Due to the infrared behavior, the result is similar to the case $\mu = 0$, $h\phi_c/T_c \ll 1$. The only difference is that the log is evaluated at T instead of $m(\phi_c)$. For a particle with large μ the contribution is

$$\eta \sim \frac{gh^4}{16\pi} \frac{m_D^2 \phi_c^2 \sigma}{\mu^3} e^{-\mu/T} \quad \text{for } \mu/T \gg 1, \quad (44)$$

which is exponentially suppressed, as expected.

In Figure 3 we have plotted the total friction coefficient (including the contributions of the top quark and gauge bosons) for the case of the SM with an additional singlet, as a function of the coupling h of the extra singlet. The dashed line corresponds to using the approximations given by Eqs. (3) and (4). Due to numerical factors in these rough approximations, this curve does not match the solid line for small h . Apart from this fact, the behavior is similar. However, for larger values of h the dashed line grows faster and crosses the solid line. This is because the approximation increases with h^4 , while the correct result does not, according to Eq. (39).

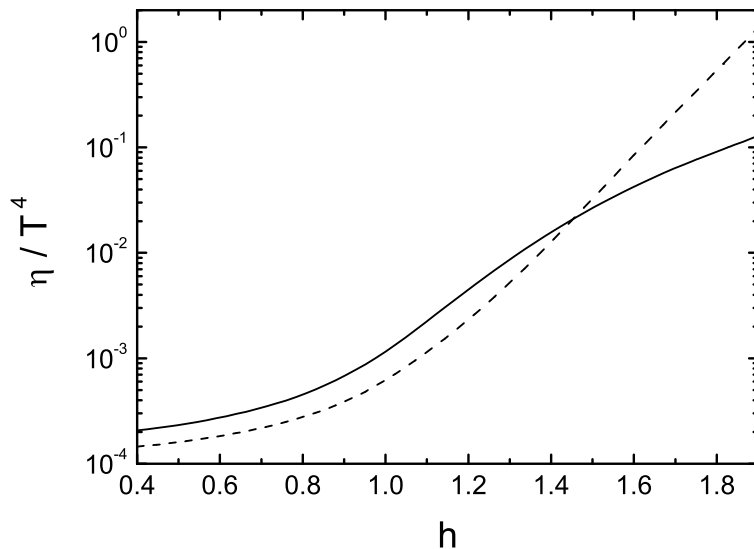


Figure 3: The friction coefficient for the SM with a complex singlet as a function of the coupling h for $m_H = 125\text{GeV}$ and $\mu = 0$ is plotted in solid line. The dashed line corresponds to using the small m/T approximations.

We wish to emphasize the fact that the friction depends on the wall profile besides depending on the parameters g and h . For instance, in the case of small m/T , η is proportional to $\phi_c^2 \sigma \sim \phi_c^4 L_w^{-1}$. Sometimes the wall width is estimated as $L_w \approx 1/T$. However, L_w may change significantly with the strength of the phase transition. We have computed L_w and σ numerically using Eqs. (19) and (20). For the parameters used in Fig. 3 they vary from $L_w \sim 100/T$ and $\sigma \sim 10^{-4}T^3$ for small h (weak phase transitions) to $L_w \sim 1/T$ and $\sigma \sim T^3$ for large h (strong phase transitions). This dependence will become particularly important if the strength of the phase transition is varied without changing the particle content of the model (e.g., by changing the tree-level potential).

4 The bubble wall velocity

If we ignore hydrodynamics, the steady state velocity of the bubble wall is obtained by equating the friction force (23) to the pressure difference between phases. We shall use subindexes b and u for quantities in the broken and unbroken symmetry phase, respectively. Thus, ignoring hydrodynamics, we have $\eta v_w = p_b(T) - p_u(T)$. Here, the pressure difference $\Delta p(T) = p_b(T) - p_u(T)$ is given by the effective potential (12), $\Delta p(T) = -V(\phi_m(T), T)$. However, the motion of the wall in the plasma causes variations of the temperature and velocity of the fluid, and is in turn affected by these perturbations.

For hydrodynamic considerations (see, e.g., [30, 31, 33]) we can assume a thin wall, and the temperature and fluid velocity turn out to be discontinuous at the interface. Thus, we have different temperatures T_u and T_b on each side of the wall. We assume a planar wall in stationary motion in the z direction. In the rest frame of the wall, the continuity conditions for energy and momentum fluxes give the relations [31]

$$\begin{aligned} w_u \gamma_u^2 v_u &= w_b \gamma_b^2 v_b, \\ w_u \gamma_u^2 v_u^2 + p_u &= w_b \gamma_b^2 v_b^2 + p_b, \end{aligned} \quad (45)$$

where v is the fluid velocity $\gamma = 1/\sqrt{1-v^2}$, and $w = \rho + p$ is the enthalpy density. In Eq. (45) we have, e.g., $p_u \equiv p_u(T_u)$ (notice that the thermodynamical quantities have in general different values in each phase, even for $T_u = T_b$). To obtain a macroscopic equation involving the friction, one can introduce a damping term of the form $u^\mu \partial_\mu \phi$ in the equation of motion for the Higgs field. This equation must be integrated taking into account the temperature variation. Assuming a thin wall, one obtains [21]

$$p_u - p_b - \frac{1}{2}(s_u + s_b)(T_u - T_b) + \frac{\eta}{2}(v_u \gamma_u + v_b \gamma_b) = 0, \quad (46)$$

where s is the entropy density and η is the friction coefficient obtained from the microphysics calculation, $\eta = [\Delta p(T)/v_w]_{\text{micro}}$. The thermodynamical variables are related by an equation of state (EOS), so Eqs. (45) and (46) have only four unknowns, namely, the velocities $v_{u,b}$ and the temperatures $T_{u,b}$. Besides, the temperature T_u outside the bubble can be determined by computing the nucleation temperature.

The velocities v_u and v_b of the fluid are measured in the reference frame of the wall. Equivalently, $|v_u|$ and $|v_b|$ give the velocity of the wall with respect to the fluid on each side of the wall. We want to calculate the wall velocity v_w in the reference frame in which the fluid is at rest *very far* in front of the

wall and very far behind the wall (at the center of the bubble). We shall refer to this reference frame as the laboratory frame.

The stationary motion of the wall admits two kinds of solutions, called detonations and deflagrations. For detonations we have $|v_b| < |v_u|$ and $|v_u| > c_s$, where $c_s = 1/\sqrt{3}$ is the speed of sound in the relativistic fluid. Therefore, in this case the wall moves supersonically with respect to the fluid in front of it. Hence, no information on the motion of the wall is transmitted into this fluid, which can be assumed to be at rest in the laboratory frame. According to this boundary condition, the detonation is supersonic, $v_w = -v_u > c_s$, and the temperature T_u is the nucleation temperature T_n . In the reference frame of the wall, the incoming flow is supersonic. The outgoing flow inside the bubble has a lower velocity and could in principle be subsonic (strong detonation). This possibility, however, is forbidden by the boundary condition at the center of the bubble. Therefore a detonation can only be weak ($|v_b| > c_s$) or Jouguet ($|v_b| = c_s$). In general, though, we will only have weak detonations [21].

For deflagrations we have $|v_b| > |v_u|$ and $|v_u| < c_s$, so the wall is subsonic with respect to the fluid in front of it. It turns out that a single front is not enough to satisfy the boundary conditions in this case. Thus, the phase-transition front must be preceded by a shock front. In the laboratory frame, the fluid between the two fronts has a finite velocity, and outside this region the fluid is at rest. Therefore, we have $v_w = -v_b$, and the fluid in front of the wall moves in the direction of the latter. In the frame of the wall, there is a subsonic flow coming from the symmetric phase, and an outgoing flow with a larger velocity v_w . In principle, the outgoing flow can be supersonic (strong deflagration), although in general we will have $v_w < c_s$ (weak deflagration). The case $v_w = c_s$ is called a Jouguet deflagration. In the deflagration case, the temperature T_u is higher than T_n , since the fluid in the region between the bubble wall and the shock front is compressed and reheated. The relation between T_u and T_n can be obtained by considering the fluid conditions (45) for the shock front [31].

In order to solve Eqs. (45) and (46), it is convenient to use the bag equation of state

$$\begin{aligned} \rho_u(T) &= a_u T^4 + \varepsilon, & p_u(T) &= a_u T^4/3 - \varepsilon, \\ \rho_b(T) &= a_b T^4, & p_b(T) &= a_b T^4/3, \end{aligned} \quad (47)$$

which is the simplest EOS that keeps the essential features of a phase transition. The coefficients a_u and a_b must be different, since in this model we have $a_b/a_u = 1 - 3\alpha_c$, with $\alpha_c \equiv \varepsilon/(a_u T_c^4)$. The constant ε is the false vacuum energy density of the high-temperature phase, and also determines the latent

heat $L \equiv \rho_u(T_c) - \rho_b(T_c)$ by³

$$L = 4\varepsilon. \quad (48)$$

In the general case, the latent heat and the vacuum energy density will not have this simple relation. In order to apply the results of this calculation to a general model, it is convenient to rewrite the parameter α_c as

$$\alpha_c = \frac{L}{4\tilde{\rho}_u(T_c)}, \quad (49)$$

where $\tilde{\rho}_u(T) = a_u T^4$ is the *thermal* energy density in the high-temperature phase.

Using the EOS (47) in Eqs. (45) and (46), we eliminate T_b ,

$$\frac{T_b}{T_u} = \left[\frac{a_u}{a_b} \left(1 - \alpha_u \frac{1 + v_u v_b}{1/3 - v_u v_b} \right) \right]^{1/4}, \quad (50)$$

where $\alpha_u \equiv \varepsilon / (a_u T_u^4)$, and we still have two equations for v_u , v_b and α_u . One of them comes from hydrodynamics alone [18],

$$v_u = \frac{\frac{1}{6v_b} + \frac{v_b}{2} \pm \sqrt{\left(\frac{1}{6v_b} + \frac{v_b}{2}\right)^2 + \alpha_u^2 + \frac{2}{3}\alpha_u - \frac{1}{3}}}{1 + \alpha_u}, \quad (51)$$

where the + and - signs in front of the square root correspond to detonations and deflagrations, respectively. The second equation involves microphysics [21],

$$\frac{4v_u v_b \alpha_u}{1 - 3v_u v_b} - \frac{2}{3} \left(1 + \frac{s_b}{s_u} \right) \left(1 - \frac{T_b}{T_u} \right) + \frac{2\alpha_u \eta}{L} (|v_u| \gamma_u + |v_b| \gamma_b) = 0, \quad (52)$$

with $s_b/s_u = (a_b/a_u) (T_b/T_u)^3$. In the case of detonations, we can solve these equations for $|v_u| = v_w$ as a function of α_u , since α_u depends on $T_u = T_n$. In the case of deflagrations, we have an additional equation relating T_u and T_n ,

$$\frac{\sqrt{3}(\alpha_n - \alpha_u)}{\sqrt{(3\alpha_n + \alpha_u)(3\alpha_u + \alpha_n)}} = \frac{v_u - v_b}{1 - v_u v_b}, \quad (53)$$

where $\alpha_n \equiv \varepsilon / (a_u T_n^4)$, and we can solve for $|v_b| = v_w$. In any case, T_u can be eliminated, and the result depends on

$$\alpha_n = \frac{L}{4\tilde{\rho}_u(T_n)}. \quad (54)$$

³A simpler model with a single coefficient $a_u = a_b = a$ is sometimes used. In that case we would have $L = \varepsilon$. However, such a model is not suitable for a phase transition, since the critical temperature [for which $p_+(T_c) = p_-(T_c)$] does not exist [21].

These equations can be solved numerically [21], and the wall velocity finally depends on the parameters α_c and α_n , and on the ratio η/L . Depending on the parameters, there may be only deflagrations, only detonations, both, or none. The deflagration solution always exists if the friction is large enough *or* the supercooling is small enough. The detonation solution will exist if the friction is small enough *and* the supercooling is large enough. In general, there is no detonation solution when the deflagration velocity is smaller than ≈ 0.5 . As the velocity approaches the speed of sound, the detonation solution may appear. The deflagration solution disappears soon after becoming supersonic. Analytical approximations were also found in Ref. [21] for both solutions. In this paper we shall use the numerical results.

Notice that the definitions of α_c and α_n [Eqs. (49) and (54)] involve the thermal energy densities at the temperatures T_c and T_n , but the latent heat is in both cases the energy density discontinuity at $T = T_c$. These parameters arise as a consequence of the use of the simple bag EOS, and their definitions must be respected in applications. As discussed in Ref. [21], if we used for α_n the energy density that is released at $T = T_n$, which is larger than L , we would be overestimating the velocity, since this would be equivalent to considering a stronger supercooling [i.e., a smaller value of $\tilde{\rho}_u(T_n)$].

5 The electroweak wall velocity

In this section we calculate the value of the wall velocity in the electroweak phase transition. For that aim, we compute the parameters α_c , α_n , and η/L for several models. The temperature T_n is defined through Eq. (16), and is the temperature at which bubbles begin to nucleate. By the time bubbles occupy all space, the temperature will be in general different. If the wall velocity is relatively large, bubbles will not have time to interact with each other until they percolate. In this case the temperature will just decrease due to the expansion of the Universe, and the velocity will increase during the phase transition. In general, though, the transition will be short enough, so that the velocity will not change significantly from $v_w(T_n)$ [32]. On the other hand, in the case of slow deflagrations, the supersonic shock fronts preceding the walls will cause a reheating during bubble expansion. Hence, the temperature will grow and the wall velocity will decrease from $v_w(T_n)$. Depending on the amount of latent heat, the reheating temperature may be very close to T_c [22, 27, 33]. In this case, the wall velocity will decrease significantly. We shall not take into account this possibility in the present paper. We remark, though, that it may have important consequences [33, 34].

We shall consider several extensions of the SM. The relevant SM contri-

butions to the one-loop effective potential come from the Z and W bosons, the top quark, and the Higgs and Goldstone bosons. It is usual to ignore the Higgs sector in the one-loop radiative corrections. This should be a good approximation in extensions of the SM which include particles with strong couplings to ϕ . The ϕ -dependent masses of the weak gauge bosons and top quark are of the form $h_i\phi$, with $h_i = m_i/v$, where m_i are the physical masses at zero temperature. We shall ignore, as usual, the longitudinal components of the weak gauge bosons, which are screened by plasma effects. Thus, the W and Z contribute corrections of the form (6,9) to the free energy (8), with 4 and 2 bosonic d.o.f., respectively. The top contributes with $g_t = 12$ fermionic d.o.f. The rest of the SM particles have $h_i \ll 1$ and only contribute a ϕ -independent term $-\pi^2 g_{\text{light}} T^4/90$, with $g_{\text{light}} \approx 90$. To strengthen the electroweak phase transition, extra particles are usually added to the SM, with strong couplings to ϕ .

5.1 SM extensions with scalars

It is well known that the easiest way of strengthening the phase transition is by extending the scalar sector of the SM. The simplest extension consists of adding gauge singlet scalars [23, 35].

5.1.1 A complex singlet

We shall first consider a model in which a single complex scalar S is added to the SM [36, 37, 38]. The coupling to the Higgs is of the form $2h^2 S^\dagger S H^\dagger H$, and the field S may have a $SU(2) \times U(1)$ invariant mass term $\mu^2 S^\dagger S$ and a quartic term $\lambda_S (S^\dagger S)^2$. For simplicity, we will ignore the possibility that cubic terms exist in the tree-level potential, and we will assume $\mu^2 \geq 0$. We notice however that a negative value of μ^2 , as well as a cubic coupling, may enhance the strength of the phase transition through tree-level effects [36]. We shall study the effect of a cubic term at the end of this section. Hence, the field S gives contributions to the free energy of the form (6,9), with $g = 2$ d.o.f. and a mass $m^2(\phi) = h^2\phi^2 + \mu^2$. The thermal mass is given by $\Pi = (h^2 + \lambda_S) T^2/3$ [37]. We shall take $\lambda_S = 0$ for our numerical calculations. We have checked that considering $\lambda_S \neq 0$ does not introduce qualitative differences in the results.

Figure 4 shows the value of the wall velocity at the nucleation temperature T_n , as a function of the coupling h for different values of the parameters. We have plotted both the deflagration and the detonation solutions, when they exist, for the case $\mu = 0$ (which maximizes the strength of the phase transition) and Higgs masses $m_H = 100, 125, 150$ and 175 GeV , and for the

case $\mu = 100\text{GeV}$ and $m_H = 125\text{GeV}$. For the same h , larger values of m_H give weaker phase transitions and, consequently, lower values of v_w . The crosses indicate the points where $\phi(T_n)/T_n = 1$. As h is increased, the phase transition becomes stronger. As a consequence, the temperature T_n decreases and the supercooling stage lasts longer. In this model, if h is too large the Higgs VEV remains stuck in the symmetric phase, and the Universe enters a period of inflation. We are not interested in such extreme cases, and we just plot the curves up to a value of h for which the time required to get out of the supercooling stage becomes too long for the numerical computation.

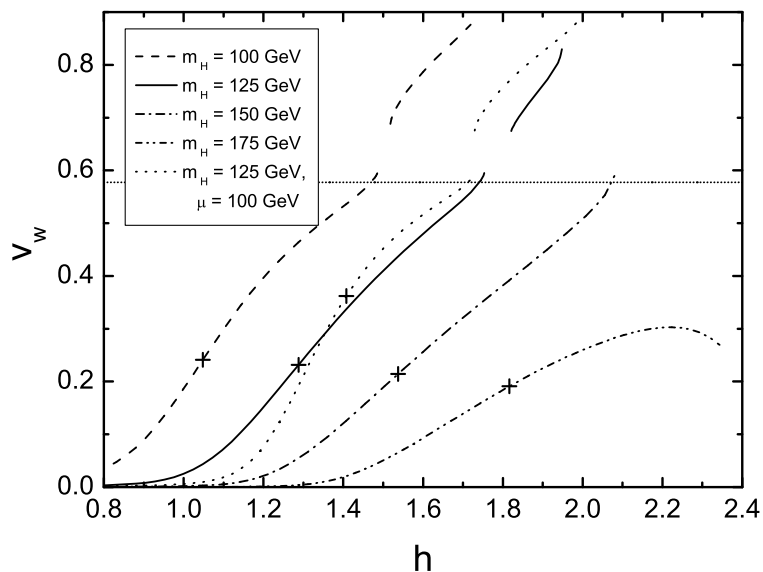


Figure 4: The wall velocity as a function of the coupling h of the singlet, for several Higgs masses. All the curves correspond to the case $\mu = 0$, except for the dotted line, which corresponds to $\mu = 100\text{GeV}$. The crosses indicate the case $\phi_n/T_n = 1$.

Although the amount of supercooling grows with h , so does the friction and the behavior of the wall velocity is rather unpredictable. As can be seen in Fig. 4, the velocity in general increases with h . However, for larger values of m_H (e.g., the case $m_H = 175\text{GeV}$), the velocity eventually decreases for large h . This is because larger values of h are required to achieve a phase transition of the same strength, and the friction becomes important. Only the cases $m_H = 100$ and 125GeV have detonations (the short curves which lie above the speed of sound). Notice that there is a small range of h for which there are neither deflagrations nor detonations, i.e., no stationary solution for the wall velocity. In such a case, the steady state will not be reached, and the

wall will accelerate until the end of the phase transition. The case in which the wall velocity gets close to the speed of light may have important implications for gravitational wave generation. Such ultrarelativistic velocities have been considered recently [39] for the SM extension with singlet scalar fields, finding that “runaway” solutions exist for very strong phase transitions.

For $\mu \neq 0$ the phase transition is weaker and the amount of supercooling is lower, but the friction is lower too. As an example, consider the case $m_H = 125\text{GeV}$ and $\mu = 100\text{GeV}$ (dotted line in Fig. 4). We see that for small h the velocity is lower than in the case of $\mu = 0$, while for large h the velocity is higher. In Fig. 5 we have plotted the wall velocity as a function of μ for $m_H = 125\text{GeV}$ and $h = 1.4, 1.6$ and 1.8 . We see that for small μ the wall velocity increases with μ , indicating that the friction decreases faster than the strength of the phase transition. For large μ the velocity eventually decreases, as the extra boson decouples from the thermal plasma. For the cases $h = 1.4$ and $h = 1.6$ there are only deflagrations. The crosses in the curves indicate a phase transition with $\phi(T_n)/T_n = 1$. To the right of this point the phase transition is weaker. The value $h = 1.8$ is quite large, and there are detonations for a long range of values of μ . In this case, deflagrations appear only for $\mu \gtrsim 170\text{GeV}$. We see that there is a range of parameters for which there exist both kinds of solution for the wall propagation, and also a range in which there is no solution.

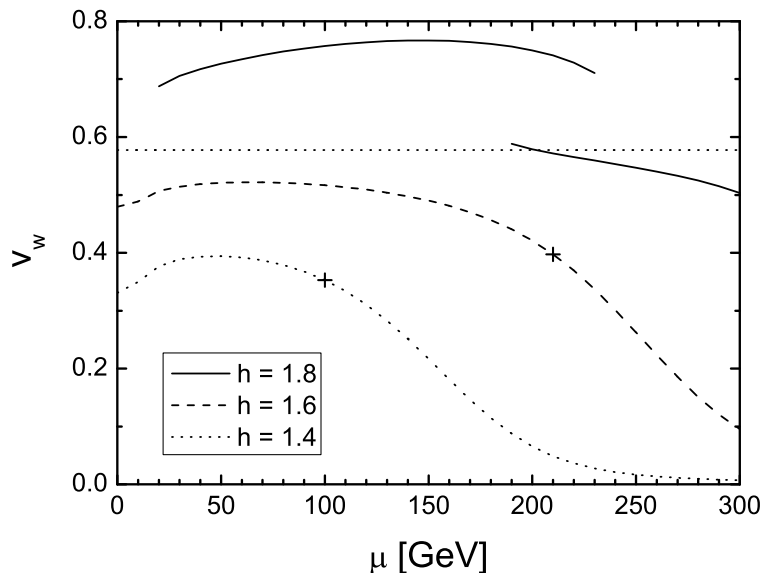


Figure 5: The wall velocity as a function of μ , for $m_H = 125\text{GeV}$ and three values of h .

5.1.2 A hidden sector

Recently, an extension of the SM with several real singlets S_i has been considered [40]. These bosons constitute a hidden sector which couples only to the SM Higgs doublet through a term $h^2 H^\dagger H \sum S_i^2$ (for simplicity, universal couplings $h_i = h$ are assumed). Following Ref. [40], we assume there are no linear, cubic, or quartic terms in the hidden-sector scalar fields. Therefore, this case is similar to the previous one, with $m^2(\phi) = h^2 \phi^2 + \mu^2$ and g d.o.f., where g is the number of singlets. We shall take $g = 12$, as in Ref. [40]. If the fields S_i do not have mass terms, so that they only get a mass from electroweak breaking, the phase transition can be made exceedingly strong. Interestingly, this model allows to consider the classically conformal case, corresponding to $m^2 = 0$ in Eq. (5). The loop corrections break conformal invariance, and a mass scale appears via dimensional transmutation. Imposing appropriate renormalization conditions, for a given Higgs mass the classically conformal case occurs for a fixed value of h . Since we are interested in the variation of the strength of the phase transition as a function of the parameters, we shall not give special attention to this particular case.

Figure 6 shows the velocity $v_w(T_n)$ as a function of the coupling h for $\mu = 0$ and different values of m_H in the range $100 - 200 GeV$. Since this model has more d.o.f. than the previous one, the phase transition becomes strongly first-order for lower values of h . As a consequence, the wall velocity grows more quickly with h . However, we see that in all the cases the nucleation stage becomes too long before detonations can exist. For $\mu \neq 0$ the phase transition weakens and higher values of h can be considered. We have found that detonations appear in the range $\mu \sim 50 - 150 GeV$ for low values of m_H and extreme values of h . For most values of h there are only deflagrations, and the behavior with μ is similar to that of the lower curves of Fig. 5.

5.2 The MSSM

The Minimal Supersymmetric Standard Model (MSSM) has been extensively investigated in connection to electroweak baryogenesis [41], since it may provide a strong phase transition and sources of CP violation. The MSSM contains two complex Higgs doublets H_1 and H_2 . We define the vacuum expectation values $v_1 \equiv \langle H_1^0 \rangle$ and $v_2 \equiv \langle H_2^0 \rangle$. It is customary to simplify the problem by considering the limit in which the CP-odd Higgs mass is large ($m_A \gg m_Z$). In this limit the low energy theory contains a single Higgs doublet Φ , and the masses and couplings depend on $\tan \beta \equiv v_2/v_1$. Thus, calling $\phi/\sqrt{2}$ the background of the real neutral component of Φ , the tree-level potential is of the form (5), with the quartic coupling given by

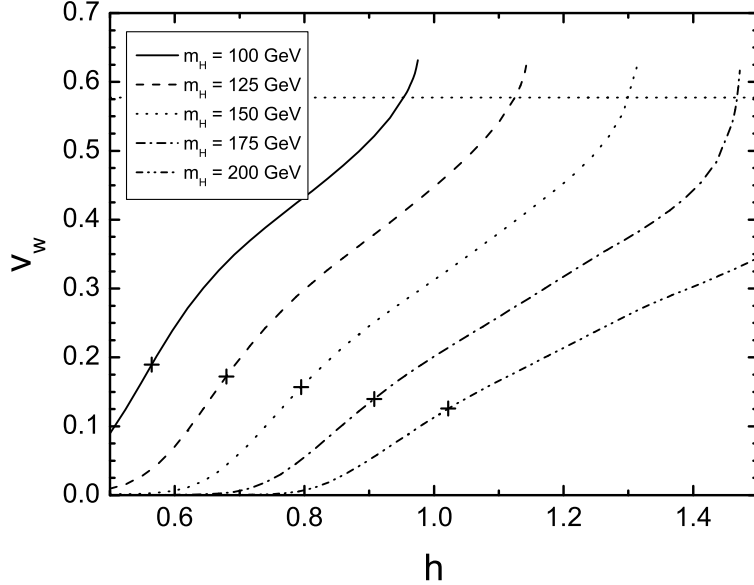


Figure 6: The wall velocity for $g = 12$ real scalars with $\mu = 0$.

$\lambda = (g^2 + g'^2) \cos^2(2\beta)/8$. Therefore, the tree-level Higgs mass is bounded by $m_H^2 < m_Z^2$. However, this tree-level relation is spoiled by radiative corrections (see e.g. [42]) and we shall consider m_H as a free parameter.

In this model, the relevant SM field-dependent masses are those of the gauge bosons,

$$m_W^2 = g^2 \phi^2 / 4 \equiv h_W^2 \phi^2, \quad m_Z^2 = (g^2 + g'^2) \phi^2 / 4 \equiv h_Z^2 \phi^2, \quad (55)$$

and top quark,

$$m_t^2(\phi) = \frac{h_t^2 \sin^2 \beta}{2} \phi^2 \equiv \bar{h}_t^2 \phi^2, \quad (56)$$

where h_t is the Yukawa coupling to H_2^0 . We shall work in the limit in which the left handed stop is heavy ($m_Q \gtrsim 500 \text{ GeV}$). In this case, the one-loop correction to the SM is dominated by the right-handed top squark contribution, with the field-dependent mass given by

$$m_{\tilde{t}}^2(\phi) \approx m_U^2 + h_{\tilde{t}}^2 \phi^2, \quad (57)$$

where

$$h_{\tilde{t}}^2 = 0.15 h_Z^2 \cos 2\beta + \bar{h}_t^2 \left(1 - \frac{\tilde{A}_t^2}{m_Q^2} \right), \quad (58)$$

m_U^2 and m_Q^2 are soft breaking parameters, and \tilde{A}_t is the stop mixing parameter. If the mass of the right-handed stop is of the order of the top mass

or below, the one-loop effective potential (12) admits the high-temperature expansion [43]

$$V(\phi, T) = D(T^2 - T_0^2)\phi^2 - T \left(E_{SM}\phi^3 + 6\frac{\mathcal{M}_{\tilde{t}}(\phi)^3}{12\pi} \right) + \frac{\lambda(T)}{4}\phi^4, \quad (59)$$

where $D = m_H^2/(8v^2) + 5h_W^2/12 + 5h_Z^2/24 + h_t^2/2$ [15], $T_0^2 = m_H^2/(4D)$, E_{SM} is the cubic-term coefficient in the high-temperature expansion for the SM effective potential, $E_{SM} \approx (2h_w^3 + h_z^3)/6\pi$, and $\mathcal{M}_{\tilde{t}}^2(\phi) = m_{\tilde{t}}^2(\phi) + \Pi_{\tilde{t}}(T)$. The thermal mass is given by [43]

$$\Pi_{\tilde{t}}(T) = \left[\frac{4g_s^2}{9} + \frac{h_t^2}{6} \left(1 + \sin^2\beta \left(1 - \frac{\tilde{A}_t^2}{m_Q^2} \right) \right) + \left(\frac{1}{3} - \frac{|\cos 2\beta|}{18} \right) g'^2 \right] T^2, \quad (60)$$

where g_s is the strong gauge coupling. Following Ref. [15], we shall set $\tilde{A}_t = 0$ for simplicity in the numerical calculation. We shall also take $\sin^2\beta = 0.8$.

The phase transition strength is maximized for negative values of the soft mass squared $m_U^2 \approx -\Pi_{\tilde{t}}(T)$ [44], for which the contribution of the term $\mathcal{M}_{\tilde{t}}^3$ in (59) is of the form $-E_{MSSM}T\phi^3$, with a coefficient E_{MSSM} that may be one order of magnitude larger than that of the SM. This would make the phase transition sufficiently strong for baryogenesis for Higgs masses as large as 100GeV . However, such large negative values of m_U^2 may induce the presence of color breaking minima at zero or finite temperature [45]. Demanding the absence of such dangerous minima constrains the Higgs mass to unrealistic values. Nevertheless, the two-loop corrections are very important and can make the phase transition strongly first-order even for $m_U \approx 0$ [46]. The most important two-loop corrections are of the form $\phi^2 \log \phi$ and are induced by the SM weak gauge bosons, as well as by stop and gluon loops [46, 47]. In the case of a heavy left-handed stop we have [43]

$$V_2(\phi, T) \approx \frac{\phi^2 T^2}{32\pi^2} \left[\frac{51}{16} g^2 - 3 \left(2\bar{h}_t^2 \left(1 - \frac{\tilde{A}_t^2}{m_Q^2} \right) \right)^2 + 8g_s^2 2\bar{h}_t^2 \left(1 - \frac{\tilde{A}_t^2}{m_Q^2} \right) \right] \log \left(\frac{\Lambda_H}{\phi} \right), \quad (61)$$

where the scale Λ_H depends on the finite corrections and is of order 100GeV . Following [15], we will set $\Lambda_H = 100\text{GeV}$ for the numerical computation, given the slight logarithmic dependence of V_2 on Λ_H .

The phase transition takes place at some temperature between the critical temperature T_c and the temperature at which the barrier between minima

disappears. The latter is approximately given by the parameter T_0 in Eq. (59). In order to avoid the presence of color-breaking minima, we only consider values of m_V^2 for which $m_V^2 + \Pi_{\tilde{t}}(T_0) > 0$ [15]. For the computation of the temperature T_n we used the high-temperature approximation (59) for the one-loop effective potential, together with the two-loop correction (61). Therefore, for the friction coefficient we also used the high-temperature approximation, given by Eqs. (3) and (4). For the stop contribution we have $m_D \sim m_{\tilde{t}} \sim h_{\tilde{t}} T$.

Figure 7 shows the wall velocity as a function of the stop mass for Higgs masses $m_H = 100, 110, 120, 130$ and 140 GeV . In the lower curve ($m_H = 140 \text{ GeV}$), the cross marks the case $\phi_n/T_n = 1$. To the right of the cross the phase transition is weak. As can be seen, for this model the velocity is not very sensitive to the stop and Higgs masses. We only obtain deflagrations, with velocities in the range $v_w \sim 0.3 - 0.45$.

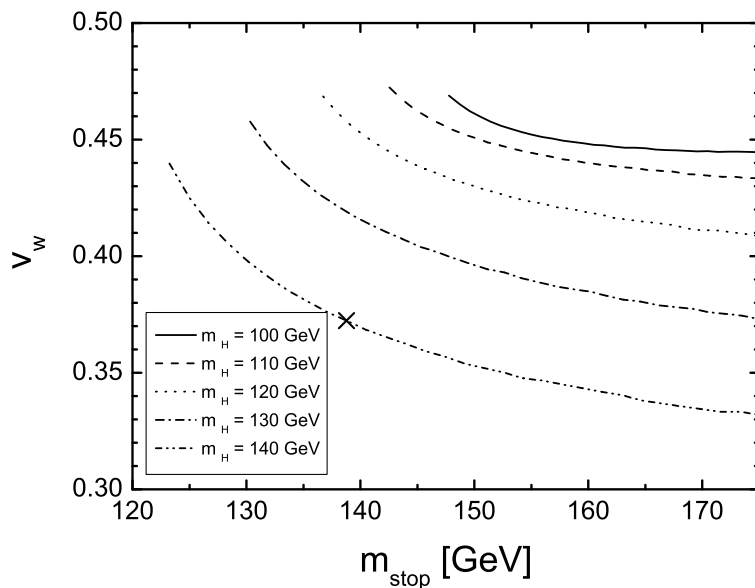


Figure 7: The wall velocity as a function of the stop mass for several Higgs masses. The cross in the lower curve marks the point of $\phi_n/T_n = 1$.

5.3 TeV fermions

So far we have considered extensions of the SM for which the relevant contributions to the effective potential came from new scalars. In Ref. [48], it was shown that in extensions with extra fermions strongly coupled to the Higgs field, the phase transition may be sufficiently strong to avoid erasure

of the baryon asymmetry in the broken-symmetry phase. Strongly coupled fermions, however, make the vacuum unstable unless the Higgs is heavy. In the model considered in Ref. [48], this problem was solved by adding heavy bosons with similar couplings and number of degrees of freedom, but with a large ϕ -independent mass term, so that they are decoupled from the dynamics at $T \sim v$. The model can be considered as a particular realization of split supersymmetry, where the standard relations between the Yukawa and gauge couplings are not fulfilled. Therefore, the fermions are higgsinos and gauginos, with a total of 16 d.o.f.

Depending on the values of the Yukawa couplings and of the mass parameters, the mass eigenvalues can be rather cumbersome. In the simplest case, only $g = 12$ d.o.f. are coupled to the SM Higgs, with degenerate eigenvalues of the form $m_f^2(\phi) = \mu^2 + h^2\phi^2$. One can assume for simplicity that the bosonic stabilizing fields have the same number of d.o.f., and a dispersion relation $m_S^2(\phi) = \mu_S^2 + h^2\phi^2$. We shall also assume, as in Ref. [48], that $\Pi_S = 0$. The maximum value of μ_S consistent with stability is obtained by requiring the quartic term in Eq. (6) to be positive at scales much larger than v . Taking into account only the radiative corrections associated with the strongly coupled fields, one finds that μ_S^2 must be below the value

$$\mu_S^2 = \exp\left(\frac{m_H^2 8\pi^2}{gh^4 v^2}\right) m_f^2(v) - h^2 v^2. \quad (62)$$

In order to minimize the effect of the stabilizing bosons on the strength of the phase transition, we will set μ_S to this maximum value. Notice, however, that we have $\mu_S \gg \mu$ only for small h , so in general the stabilizing bosons are not completely decoupled from the thermal plasma.

In Fig. 8 we have plotted the wall velocity for $\mu_f = 0$ and different values of m_H . The parts of the curves on the right of the crosses correspond to $\phi(T_n)/T_n > 1$. To obtain a strongly first-order phase transition with extra fermions, large values of the Yukawa coupling h are needed. Therefore, the friction coefficient is in general larger than in models in which the strength of the transition is enhanced with extra bosons. As a consequence, the wall velocity is smaller. We find velocities $v_w \lesssim 0.25$, and as small as $v_w = 0.05$ for strongly first-order phase transitions. This makes this model interesting for baryogenesis, since the generated baryon asymmetry peaks for $v_w \ll 1$ [4, 5]. Figure 9 shows the case $\mu \neq 0$, for $m_H = 125\text{GeV}$ and different values of h . In the lower curves, the phase transition is weak on the right of the crosses. We see that the wall velocity can either grow or decrease as the invariant mass of the extra particles is increased. Nevertheless, v_w is still in the range $0.05 \lesssim v_w \lesssim 0.25$ for strongly first-order transitions.

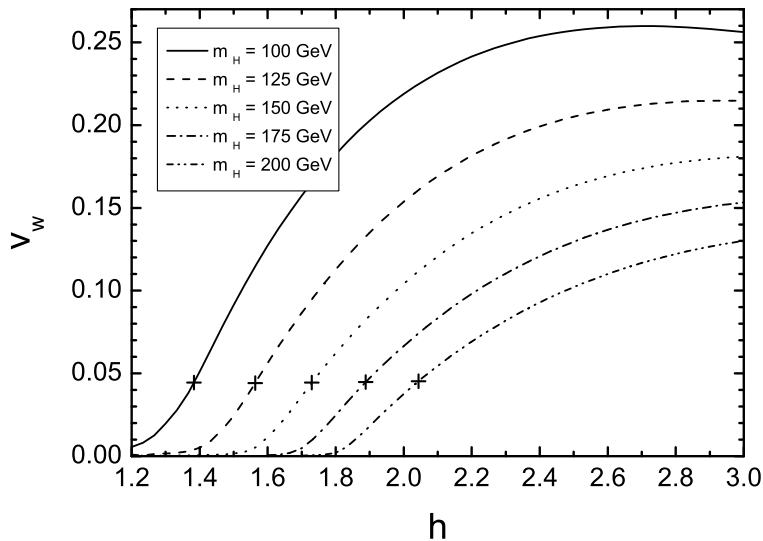


Figure 8: The wall velocity as a function of h , for $g = 12$ and $\mu = 0$. The points to the right of the crosses correspond to phase transitions with $\phi_n/T_n > 1$.

5.4 Other extensions

Given the large variety of extensions of the SM, it is not feasible to consider all the models. For many models, the strength of the phase transition depends only on the particle content. Generally, adding bosons to the SM makes the phase transition more strongly first-order, whereas fermions make it weaker. To one-loop order, the magnitude of this effect depends on the coupling of the extra particles to the Higgs boson, as well as on their number of degrees of freedom. The friction also depends on these parameters, increasing with the addition of either bosons or fermions. The previous examples correspond to such models, in which the extra-SM sector was dominated either by bosons or by fermions. For an intermediate model in which bosons and fermions have the same values of g , h , and μ , we have obtained intermediate values of the velocity, namely, only deflagrations with $v_w \sim 0.15 - 0.35$ for phase transitions with $\phi_n/T_n > 1$.

On the other hand, the strength of the phase transition may be changed without directly changing the particle content of the model. This is what happens, e.g., in the MSSM when the two-loop contribution (61) is taken into account. Another possibility is the introduction of a non-renormalizable dimension-six term of the form $(\Phi^\dagger\Phi - v^2/2)^3/\Lambda^2$ in the Higgs potential, which allows to consider a negative quartic coupling [49]. Adding a real singlet field S to the SM allows for the possibility of cubic terms of the form

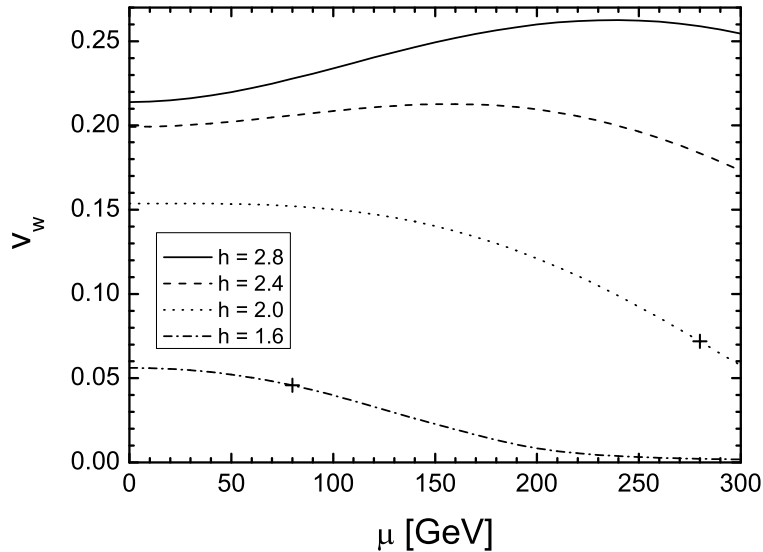


Figure 9: The wall velocity as a function of h , for $g = 12$ and $m_H = 125\text{GeV}$. For the points to the right of the crosses the phase transition is weak ($\phi_n/T_n < 1$).

$(H^\dagger H)S$ or S^3 in the tree-level potential, which cannot be constructed with Higgs doublets. The presence of cubic terms already at zero temperature makes it easier to get a strongly first-order electroweak phase transition [36]. This possibility exists also in the Next to Minimal Supersymmetric Standard Model (NMSSM), which consists of adding a gauge singlet to the MSSM. In this model the cubic terms arise as supersymmetry-breaking soft terms. Since the strength of the transition is dominated by the cubic terms in the tree-level potential, it is not necessary to rely on loop corrections or to consider a light stop [50].

In these modifications of the SM, the phase transition can be made strongly first-order without increasing the friction. In order to explore the effect of such a tree-level modification on the wall velocity, we shall consider the addition of cubic terms. Considering the full potential makes the model considerably more complicated than those we have studied so far, since one has to deal with more than one scalar and several free parameters. Instead, we shall consider a toy model which consists of adding a term $-A\phi^3$ to the tree-level potential (5) for the SM, where A is a free parameter with mass dimensions. In this model the parameters of the potential are related to the physical Higgs VEV and mass by $2m^2 = \lambda v^2 - 3Av$, $m_H^2 = 2\lambda v^2 - 3Av$. We

shall use the high-temperature potential

$$V(\phi, T) = D_{SM} (T^2 - T_0^2) \phi^2 - (TE_{SM} + A) \phi^3 + \frac{\lambda}{4} \phi^4, \quad (63)$$

with the SM values given by $D_{SM} = (2h_W^2 + 2h_t^2 + h_Z^2)/8$, $E_{SM} = (2h_W^3 + h_Z^3)/6\pi$, and $T_0^2 = m^2/D_{SM}$.

We show the results in Fig. 10. We have considered values of the parameters for which $h_t\phi/T \lesssim 1$, so that the high-temperature expansion (63) is valid. The strength of the phase transition increases very quickly with A , and this is reflected in the behavior of the wall velocity. Notice that, although in this case the particle content does not change, the friction coefficient increases with the strength of the transition due to its dependence on the surface tension. Eventually, the wall velocity stops growing. There is also a strong dependence on m_H . For smaller values of m_H ($m_H = 100$ and 200GeV) the strengthening with A is so fast that the deflagration solution quickly becomes supersonic and disappears. In these cases, the detonation solution does not appear before the phase transition ceases to occur. Interestingly, detonations appear for weaker phase transitions (higher values of m_H).

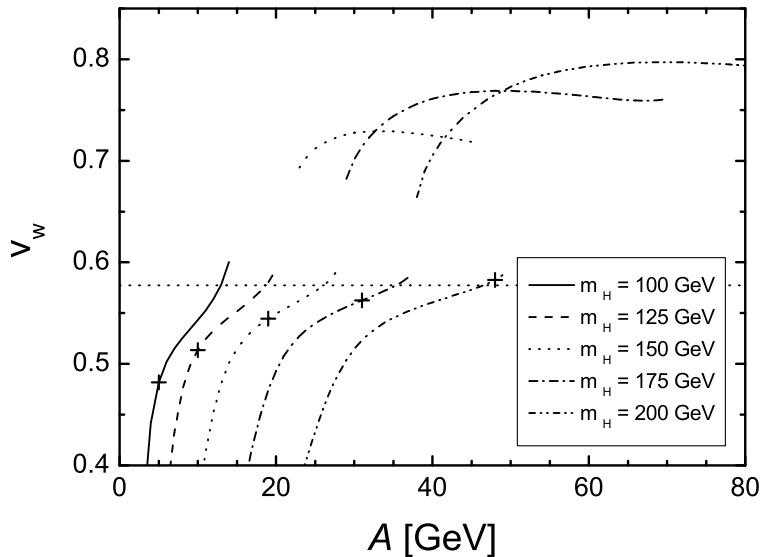


Figure 10: The wall velocity for the SM with a cubic term $-A\phi^3$.

6 Gravitational waves and baryogenesis

The generation of gravitational waves and of the baryon asymmetry of the Universe in the electroweak phase transition seem to be mutually exclusive, since baryogenesis requires small wall velocities while GW production requires large velocities. In this section we discuss which of them is more likely in the various extensions of the SM we have considered.

Both detonations and deflagrations generate gravitational waves [1, 2, 11, 12, 13, 14, 15, 16, 17, 51, 52]. However, higher velocities give stronger signals, and Jouguet detonations are often assumed for studying GW generation. As shown in Ref. [21], the Jouguet velocity is not a good approximation and detonations, when they exist, are weak detonations. Furthermore, as we have seen, in the case of the electroweak phase transition detonations exist only in some of the extensions of the SM, and for extreme values of the parameters, namely, small Higgs masses and large coupling h . (Interestingly, a non-vanishing mass parameter μ may favor the appearance of detonations, as can be seen in Fig. 4). In any case, detonations are more likely in models in which the strength of the transition is enhanced by tree-level effects, as shown in Fig. 10. On the other hand, deflagrations with $v_w \gtrsim 0.1$ may also produce a signal of GWs observable by LISA [52]. We remark that the usual assumption that detonations are a stronger source of GWs than deflagrations may be wrong. Weak detonations have larger velocities than Jouguet detonations, but cause a smaller disturbance in the fluid. On the other hand, deflagrations with velocities close to c_s may cause important perturbations. For most of the models we have considered, there is a wide range of parameters for which the deflagration velocity is quite large. Extensions of the SM with strongly coupled fermions constitute the only exception.

For the baryon asymmetry of the Universe to be produced at the electroweak phase transition, the latter must be *strong enough*, i.e., the condition $\phi/T > 1$ must be fulfilled. On the other hand, the generated BAU is maximized for velocities $v_w \lesssim 10^{-1}$, and is strongly suppressed for higher velocities. This condition demands a *weak enough* phase transition, how weak depending on the friction. These two conditions may restrict significantly the parameters of the theory. Models with extra bosons which are strongly coupled to the Higgs have been extensively considered, since they easily give strongly first-order phase transitions. However, in our examples we have seen that these models also tend to give quite large wall velocities. For extensions with scalar singlets, we obtained in all the cases $v_w \gtrsim 0.2$ for $\phi_n/T_n \geq 1$, and even larger ($v_w \gtrsim 0.5$) if tree-level cubic terms are allowed. For the MSSM with a light stop we also obtained rather large velocities, $v_w \gtrsim 0.35$. On the other hand, extensions with fermions are not usually taken into account

because they tend to weaken the phase transition. However, models with fermions can give strong enough phase transitions, as shown in Ref. [48] for the case of fermions with large Yukawa coupling h and heavier stabilizing bosons. For this model, with μ_S given by Eq. (62), we see that the wall velocity can be as small as $v_w = 5 \times 10^{-2}$ for $\phi_n/T_n = 1$ (see Figs. 8 and 9).

Due to the approximations used in the calculation of the friction coefficient, the error in the wall velocity is an $\mathcal{O}(1)$ factor. With a larger friction, extensions with bosons may give velocities $v_w \lesssim 0.1$ for $\phi_n/T_n = 1$. In any case, it is clear that values of ϕ_n/T_n and v_w which are appropriate for baryogenesis are more easily obtained in models in which the dynamics is dominated by fermions. If the friction is smaller than our estimate, we will have higher velocities, which favors the generation of GWs. For instance, in the MSSM, if we consider a friction coefficient a factor of 3 smaller we obtain deflagrations with $v_w \approx c_s$ and detonations with $v_w \approx 0.85$ for $m_H = 120\text{GeV}$.

7 Conclusions

We have studied the velocity of bubble walls in the electroweak phase transition. We have estimated the friction on the wall due to particles with dispersion relation $m^2 = \mu^2 + h^2\phi^2$, for arbitrary values of the parameters μ and h . We have discussed analytically the cases of small and large μ/T and $h\phi/T$. We have solved numerically the equations for the wall velocity, taking into account the friction and the hydrodynamics, and we have computed the electroweak wall velocity for several extensions of the Standard Model. We have also discussed the implications of our results for baryogenesis and gravitational wave generation.

The friction coefficient, as well as the amount of supercooling, have a strong, nontrivial dependence on the coupling h of the particles to the Higgs. Furthermore, the friction depends on the bubble wall profile, and thus on the strength of the phase transition. Therefore, the wall velocity is not related to the strength of the transition in a simple way, and the behavior depends on the model. We have found that in general the velocity increases with the coupling h , but it can also decrease (see, e.g., Fig. 4). As we increase the mass parameter μ , the friction tends to increase for small μ and to decrease for large μ .

As we have seen, detonations exist only for high values of h and low values of m_H , except in the case in which the strength of the phase transition is due to tree-level effects rather than to loop contributions of extra particles. We stress that there may be $\mathcal{O}(1)$ errors in our estimate of the friction coefficient. For non-relativistic velocities this will not introduce qualitative differences.

However, if a model has deflagrations with velocity close to the speed of sound, a lower friction may cause the detonation solution to exist and the deflagration to disappear. In particular, the interaction rates Γ need to be calculated accurately in each model.

We have also seen that it is difficult to obtain small velocities in phase transitions with $\phi_n/T_n \geq 1$. For instance, the MSSM gives velocities in the range $0.35 \lesssim v_w \lesssim 0.45$, a hidden sector of scalar singlets gives velocities ranging from $v_w \gtrsim 0.1$ up to supersonic values, and a tree-level cubic term causes velocities $v_w \gtrsim 0.5$. In these models the wall velocity is rather large for baryogenesis. On the other hand, such high velocities (either detonations or deflagrations) may produce an observable signal of GWs. In contrast, the presence of fermions causes smaller velocities, since they increase the friction without increasing the phase transition strength. Thus, baryogenesis is more likely in models with fermions. In particular, for the model considered in Ref. [48], which contains fermions with large Yukawa couplings h , we have found velocities in the range $0.05 \lesssim v_w \lesssim 0.25$ for $\phi_n/T_n \geq 1$.

Acknowledgements

This work was supported in part by Universidad Nacional de Mar del Plata, Argentina, grants EXA 365/07 and 425/08. The work by A.D.S. was supported by CONICET through project PIP 5072. The work by A.M. was supported by CONICET through project PIP 112-200801-00943.

References

- [1] M. Kamionkowski, A. Kosowsky and M. S. Turner, Phys. Rev. D **49**, 2837 (1994).
- [2] A. Kosowsky, A. Mack and T. Kahniashvili, Phys. Rev. D **66**, 024030 (2002).
- [3] For reviews, see A. G. Cohen, D. B. Kaplan and A. E. Nelson, Ann. Rev. Nucl. Part. Sci. **43**, 27 (1993) [arXiv:hep-ph/9302210]; A. Riotto and M. Trodden, Ann. Rev. Nucl. Part. Sci. **49**, 35 (1999) [arXiv:hep-ph/9901362].
- [4] B. H. Liu, L. D. McLerran and N. Turok, Phys. Rev. D **46**, 2668 (1992); N. Turok, Phys. Rev. Lett. **68**, 1803 (1992).

- [5] A. E. Nelson, D. B. Kaplan and A. G. Cohen, Nucl. Phys. B **373**, 453 (1992). J. M. Cline and K. Kainulainen, Phys. Rev. Lett. **85**, 5519 (2000) [arXiv:hep-ph/0002272]; J. M. Cline, M. Joyce and K. Kainulainen, JHEP **0007**, 018 (2000) [arXiv:hep-ph/0006119]; M. Carena, J. M. Moreno, M. Quiros, M. Seco and C. E. Wagner, Nucl. Phys. B **599**, 158 (2001) [arXiv:hep-ph/0011055].
- [6] G. D. Moore and T. Prokopec, Phys. Rev. D **52**, 7182 (1995) [arXiv:hep-ph/9506475]; Phys. Rev. Lett. **75**, 777 (1995) [arXiv:hep-ph/9503296].
- [7] P. John and M. G. Schmidt, Nucl. Phys. B **598**, 291 (2001) [Erratum-ibid. B **648**, 449 (2003)].
- [8] M. Dine, R. G. Leigh, P. Y. Huet, A. D. Linde and D. A. Linde, Phys. Rev. D **46**, 550 (1992) [arXiv:hep-ph/9203203].
- [9] S. Y. Khlebnikov, Phys. Rev. D **46**, 3223 (1992); P. Arnold, Phys. Rev. D **48**, 1539 (1993) [arXiv:hep-ph/9302258].
- [10] G. D. Moore, JHEP **0003**, 006 (2000).
- [11] A. D. Dolgov, D. Grasso and A. Nicolis, Phys. Rev. D **66**, 103505 (2002).
- [12] C. Caprini and R. Durrer, Phys. Rev. D **74**, 063521 (2006).
- [13] T. Kahniashvili, A. Kosowsky, G. Gogoberidze and Y. Maravin, Phys. Rev. D **78**, 043003 (2008) [arXiv:0806.0293 [astro-ph]]; T. Kahniashvili, L. Kisslinger and T. Stevens, arXiv:0905.0643 [astro-ph.CO].
- [14] S. J. Huber and T. Konstandin, arXiv:0806.1828 [hep-ph].
- [15] R. Aureda, M. Maggiore, A. Nicolis and A. Riotto, Nucl. Phys. B **631**, 342 (2002) [arXiv:gr-qc/0107033].
- [16] A. Nicolis, Class. Quant. Grav. **21**, L27 (2004).
- [17] C. Grojean and G. Servant, Phys. Rev. D **75**, 043507 (2007).
- [18] P. J. Steinhardt, Phys. Rev. D **25**, 2074 (1982).
- [19] M. Laine, Phys. Rev. D **49**, 3847 (1994) [arXiv:hep-ph/9309242].
- [20] P. Y. Huet, K. Kajantie, R. G. Leigh, B. H. Liu and L. D. McLerran, Phys. Rev. D **48**, 2477 (1993) [arXiv:hep-ph/9212224].

- [21] A. Megevand and A. D. Sanchez, Nucl. Phys. B **820**, 47 (2009) [arXiv:0904.1753 [hep-ph]].
- [22] A. Megevand, Phys. Rev. D **69**, 103521 (2004).
- [23] G. W. Anderson and L. J. Hall, Phys. Rev. D **45**, 2685 (1992).
- [24] M. Quiros, arXiv:hep-ph/9901312.
- [25] S. R. Coleman, Phys. Rev. D **15**, 2929 (1977) [Erratum-ibid. D **16**, 1248 (1977)]; C. G. Callan and S. R. Coleman, Phys. Rev. D **16**, 1762 (1977).
- [26] I. Affleck, Phys. Rev. Lett. **46**, 388 (1981); A. D. Linde, Nucl. Phys. B **216**, 421 (1983) [Erratum-ibid. B **223**, 544 (1983)]; Phys. Lett. B **100**, 37 (1981).
- [27] A. Megevand and A. D. Sanchez, Phys. Rev. D **77**, 063519 (2008) [arXiv:0712.1031 [hep-ph]].
- [28] G. D. Moore and N. Turok, Phys. Rev. D **55** 6538 (1997).
- [29] P. Arnold, D. Son and L. G. Yaffe, Phys. Rev. D **55**, 6264 (1997) [arXiv:hep-ph/9609481].
- [30] M. Gyulassy, K. Kajantie, H. Kurki-Suonio and L. D. McLerran, Nucl. Phys. B **237** (1984) 477; K. Enqvist, J. Ignatius, K. Kajantie and K. Rummukainen, Phys. Rev. D **45**, 3415 (1992); J. Ignatius, K. Kajantie, H. Kurki-Suonio and M. Laine, Phys. Rev. D **49**, 3854 (1994); H. Kurki-Suonio, Nucl. Phys. B **255**, 231 (1985); K. Kajantie and H. Kurki-Suonio, Phys. Rev. D **34**, 1719 (1986).
- [31] L. D. Landau and E. M. Lifshitz, *Fluid Mechanics* (Pergamon Press, New York, 1989); R. Courant and K. O. Friedrichs, *Supersonic Flow and Shock Waves* (Springer-Verlag, Berlin, 1985).
- [32] A. Megevand, Int. J. Mod. Phys. D **9**, 733 (2000) [arXiv:hep-ph/0006177].
- [33] A. F. Heckler, Phys. Rev. D **51** (1995) 405 [arXiv:astro-ph/9407064].
- [34] A. Mégevand, Phys. Rev. D **64**, 027303 (2001) [arXiv:hep-ph/0011019]; A. Mégevand and F. Astorga, Phys. Rev. D **71**, 023502 (2005); A. Megevand, Phys. Lett. B **642**, 287 (2006) [arXiv:astro-ph/0509291].

- [35] M. Dine, P. Huet, R. L. . Singleton and L. Susskind, Phys. Lett. B **257**, 351 (1991); M. Dine, P. Huet and R. L. . Singleton, Nucl. Phys. B **375**, 625 (1992).
- [36] J. Choi and R. R. Volkas, Phys. Lett. B **317**, 385 (1993) [arXiv:hep-ph/9308234]; S. W. Ham, Y. S. Jeong and S. K. Oh, J. Phys. G **31**, 857 (2005) [arXiv:hep-ph/0411352].
- [37] J. R. Espinosa and M. Quiros, Phys. Lett. B **305**, 98 (1993) [arXiv:hep-ph/9301285].
- [38] A. Ahriche, Phys. Rev. D **75**, 083522 (2007) [arXiv:hep-ph/0701192]; S. Profumo, M. J. Ramsey-Musolf and G. Shaughnessy, JHEP **0708**, 010 (2007) [arXiv:0705.2425 [hep-ph]]; A. Ashoorioon and T. Konstandin, arXiv:0904.0353 [hep-ph].
- [39] D. Bodeker and G. D. Moore, arXiv:0903.4099 [hep-ph].
- [40] J. R. Espinosa and M. Quiros, Phys. Rev. D **76**, 076004 (2007) [arXiv:hep-ph/0701145]; J. R. Espinosa, T. Konstandin, J. M. No and M. Quiros, Phys. Rev. D **78**, 123528 (2008) [arXiv:0809.3215 [hep-ph]].
- [41] A. G. Cohen and A. E. Nelson, Phys. Lett. B **297**, 111 (1992) [arXiv:hep-ph/9209245]; J. R. Espinosa, M. Quiros and F. Zwirner, Phys. Lett. B **307**, 106 (1993) [arXiv:hep-ph/9303317]; A. Brignole, J. R. Espinosa, M. Quiros and F. Zwirner, Phys. Lett. B **324**, 181 (1994) [arXiv:hep-ph/9312296]; S. Myint, Phys. Lett. B **287**, 325 (1992) [arXiv:hep-ph/9206266]; G. F. Giudice, Phys. Rev. D **45**, 3177 (1992).
- [42] J. A. Casas, J. R. Espinosa, M. Quiros and A. Riotto, Nucl. Phys. B **436**, 3 (1995) [Erratum-ibid. B **439**, 466 (1995)] [arXiv:hep-ph/9407389].
- [43] M. S. Carena, M. Quiros and C. E. M. Wagner, Nucl. Phys. B **524**, 3 (1998) [arXiv:hep-ph/9710401].
- [44] M. S. Carena, M. Quiros and C. E. M. Wagner, Phys. Lett. B **380**, 81 (1996) [arXiv:hep-ph/9603420].
- [45] M. S. Carena and C. E. M. Wagner, Nucl. Phys. B **452** (1995) 45 [arXiv:hep-ph/9408253].
- [46] J. R. Espinosa, Nucl. Phys. B **475**, 273 (1996) [arXiv:hep-ph/9604320].

- [47] J. E. Bagnasco and M. Dine, *Phys. Lett. B* **303**, 308 (1993) [arXiv:hep-ph/9212288]; P. Arnold and O. Espinosa, *Phys. Rev. D* **47**, 3546 (1993) [Erratum-ibid. *D* **50**, 6662 (1994)] [arXiv:hep-ph/9212235]; Z. Fodor and A. Hebecker, *Nucl. Phys. B* **432**, 127 (1994) [arXiv:hep-ph/9403219].
- [48] M. S. Carena, A. Megevand, M. Quiros and C. E. M. Wagner, *Nucl. Phys. B* **716**, 319 (2005) [arXiv:hep-ph/0410352].
- [49] X. m. Zhang, *Phys. Rev. D* **47**, 3065 (1993) [arXiv:hep-ph/9301277]; S. W. Ham and S. K. Oh, *Phys. Rev. D* **70**, 093007 (2004) [arXiv:hep-ph/0408324]; C. Grojean, G. Servant and J. D. Wells, *Phys. Rev. D* **71**, 036001 (2005) [arXiv:hep-ph/0407019]. B. Grinstein and M. Trott, *Phys. Rev. D* **78**, 075022 (2008) [arXiv:0806.1971 [hep-ph]].
- [50] M. Pietroni, *Nucl. Phys.* **B402** (1993) 27 [arXiv:hep-ph/9207227]; A. T. Davies, C. D. Froggatt and R. G. Moorhouse, *Phys. Lett.* **B372** (1996) 88 [arXiv:hep-ph/9603388]; S. J. Huber and M. G. Schmidt, *Nucl. Phys.* **B606** (2001) 183 [arXiv:hep-ph/0003122]; M. Bastero-Gil, C. Hugonie, S. F. King, D. P. Roy and S. Vempati, *Phys. Lett.* **B489** (2000) 359 [arXiv:hep-ph/0006198]; J. Kang, P. Langacker, T. J. Li and T. Liu, arXiv:hep-ph/0402086; A. Menon, D. E. Morrissey and C. E. M. Wagner, *Phys. Rev.* **D70** (2004) 035005 [arXiv:hep-ph/0404184]. For a recent review, see M. Maniatis, arXiv:0906.0777 [hep-ph].
- [51] C. Caprini, R. Durrer and G. Servant, *Phys. Rev. D* **77**, 124015 (2008) [arXiv:0711.2593 [astro-ph]].
- [52] A. Megevand, *Phys. Rev. D* **78** (2008) 084003 [arXiv:0804.0391 [astro-ph]].